DOI: 10.53469/jcmp.2025.07(11).03

A Model Comprising Four Cuproptosis-associated lncRNAs for Predicting the Immune Landscape and Prognosis in Cervical Cancer Patients

Gaoming Si[1], Zhaoxuan Liu[1], Hui Li[2], Hailong Shi[3], Wenting Yang[4], Zhiping Ruan[5], Benhua Song[2], Rui Xu[1,2,*]

[1]The Second Affiliated Hospital of Shaanxi University of Chinese Medicine, Shaanxi University of Chinese Medicine, Xianyang 712046, Shaanxi, China
[2]Department of Internal Medicine, Shaanxi Provincial Cancer Hospital, Xi'an 710061, Shaanxi, China
[3]School of Basic Medical Sciences, Shaanxi University of Chinese Medicine, Xianyang 712046, Shaanxi, China
[4]Department of Reproductive Medicine, The First Affiliated Hospital of the Medical College, Xi'an Jiaotong University, Xi'an 710061, Shaanxi, China
[5]Department of Medical Oncology, The First Affiliated Hospital of the Medical College, Xi'an Jiaotong University, Xi'an 710061, Shaanxi, China
**Correspondence Author*

Abstract: ***Cuproptosis, a newly discovered process of copper-dependent cellular demise, is initiated by the direct interaction of Cu^{2+} with lipoylated components within the mitochondrial tricarboxylic acid (TCA) cycle. This mechanism hinders cellular respiration and influences carcinogenesis, angiogenesis, and metastasis. The specific role of cuproptosis-related long non-coding RNAs (CRLs) in cervical cancer remains poorly understood. This research developed a predictive model using CRLs and investigated its potential molecular roles in the tumor microenvironment, as well as its influence on clinical outcomes in cervical cancer. We initially assessed putative CRLs from TCGA cervical cancer transcriptome data by linking cuproptosis regulators with lncRNA expression using Pearson correlation analysis. From 188 differentially expressed lncRNAs, univariate Cox and LASSO regression analysis developed a four-CRL prognostic model consisting of AC096992.2, MKLN1-AS, BAIAP2-DT, and LINC02356. Patients were categorized into two groups, high-risk and low-risk, based on a computed risk score. Multivariate Cox analysis, which included clinicopathological factors, confirmed substantial survival differences among these groups. Additionally, distinct profiles of immune checkpoint markers and tumor-infiltrating immune cells were discerned between the two cohorts. Our CRL model serves as an independent predictive tool for cervical cancer, deepens our understanding of CRL-mediated carcinogenesis, and provides valuable insights for the development of novel therapeutic options.***

Keywords: Cervical cancer, Cuproptosis, Immunotherapy, Prognostic signature, Tumor microenvironment.

1. Introduction

Despite advances in early detection and preventive vaccination, cervical cancer is still a common gynecological troublemaker [1-4]. Conventional prognostic markers such as FIGO stage, histological grade, and lymph node status are prevalent in clinical practice; nevertheless, they fail to correctly represent the immunological landscape or account for intratumoral heterogeneity. Moreover, their predictive value for immunotherapeutic response remains limited [5,6]. In contrast, transcriptome-derived molecular markers provide more precise patient stratification and may improve prognostic accuracy [7,8].

The presence of excess copper within cells can lead to cuproptosis, a newly identified form of programmed cell death that specifically targets lipoylated components of the tricarboxylic acid (TCA) cycle [9]. The loss of iron-sulfur cluster proteins, along with a build-up of lipoylated proteins, cranks up proteotoxic stress, ultimately leading to cell death9. This cellular apoptosis mechanism functions across diverse biological contexts and pathologies, significantly impacting the advancement and progression of numerous cancers [10]. Recent evidence indicates that cervical cancer cells undergo cuproptosis, and exploring this phenomenon may facilitate the identification of new screening biomarkers, prognostic markers, and therapeutic targets for this cancer [11,12]. Although they don't code for proteins, long non-coding RNAs (lncRNAs) — transcripts longer than 200 nucleotides — regulate a ton of cellular processes, including cell cycle regulation, differentiation, and epigenetic modifications [13-15]. LncRNAs significantly impact cancer progression, invasion, metastasis, and resistance to treatment because of their regulatory functions in proliferation and differentiation [16]. The role of cuproptosis-related lncRNAs (CRLs) in the tumor microenvironment and cervical cancer prognosis is still unclear, even though many lncRNAs are non-invasive markers for cervical cancer diagnosis, prognosis, and monitoring [17]. Therefore, a methodical examination of CRLs may offer a revolutionary viewpoint for improving prognostication and pre-therapeutic efficacy evaluation in patients with cervical cancer.

To figure out the connection between CRL signatures, patient outcome, immunotherapeutic efficacy, and the immune microenvironment, we distilled a four-CRL prognostic cassette and built a risk-prediction framework using the TCGA-CESC cohort. By multi-dimensionally analyzing this data, we hypothesize that the CRL-based risk algorithm predicts cervical cancer prognosis and provides a new tool for therapeutic improvement.

2. Materials and Procedures

2.1 Source of Patient Data

Clinical and RNA-seq metadata were obtained on 2025-07-05 from The Cancer Genome Atlas (TCGA) (https://www.cancer.gov/). Including annotated age, FIGO stage, TNM stage, overall survival (OS), and other clinicopathologic characteristics, the cohort included 306 TCGA-CESC cases. Genes linked to cuproptosis were assigned to training and testing sets of patients, which were randomly divided 5:5. The Kaplan–Meier Plotter (http://kmplot.com/analysis/index.php?) was used to conduct survival analyses. According to the TCGA publication criteria (http://cancergenome.nih.gov/publications/publicationguidelines), mRNA-seq data are unrestricted public releases and did not require extra Institutional Review Board permission. GENCODE was used to do lncRNA annotation (https://www.gencodegenes.org/).

2.2 Model Development and Verification

The limma R program was used to do differential profiling between normal and tumor samples, using an adjusted p-value threshold of 0.05 and $|logFC| > 1$ [18]. Under ten-fold cross-validation, univariate Cox and LASSO regressions using the glmnet R package were used to identify genes linked to survival [19]. Important genes and their coefficients were then retrieved using a multivariate Cox model. A risk model was created based on four CRLs, their appropriate cut-offs, and associated coefficients. The CRL risk score of every individual was calculated as follows: risk score = Σ(*Expression lncRNA i* × *Coefficient lncRNA i*).

2.3 Analysis of Consensus Clustering

The pheatmap R package was utilized to show CRL expression divergence and clinicopathologic features across clusters, while the ConsensusClusterPlus R program was utilized to divide all CESC patients into discrete clusters in order to analyze the CRL signature landscape in CESC [20]. GSVA was carried out using the c2.cp.kegg.v7.4.symbols.gmt gene set, which was curated by MsigDB, for functional interrogation.

2.4 Formulation of the Model

The survminer R program was employed to compute the median risk score, facilitating the categorization of all CESC patients into high- and low-risk groups. The generated cut-off was subsequently integrated into the model equation. Concordance was measured by the PEC program, and time-dependent ROC curve analysis assessed the forecasting capability of this model.

2.5 Separate Prognostic Evaluation and Nomogram Development

Univariate and multivariate Cox regressions were employed to ascertain whether the risk score served as an independent prognostic factor. A nomogram was created in R to assess the 1-, 3-, and 5-year survival probability for CESC patients within the TCGA cohort, using the risk score alongside clinicopathologic variables.

2.6 Analysis of Functional Enrichment

To elucidate operational annotations and enriched pathways, differentially expressed genes linked to the four CRLs in CESC underwent enrichment profiling utilizing Gene Ontology (GO) and Kyoto Encyclopedia of Genes and Genomes (KEGG).

2.7 Analyzing the Immune Risk Profile Within the Tumor Microenvironment

To evaluate immune infiltration patterns, we leveraged established computational tools—including XCELL, TIMER, QUANTISEQ, MCPcounter, EPIC, CIBERSORT, and CIBERSORT-ABS—to generate immune cell abundance scores [21-25]. Spearman correlation analysis was then applied to explore associations between immune cell populations and risk stratification. CIBERSORT-derived signatures were employed to further classify CESC patients into immunological subgroups. A panel of twenty potentially targetable immune checkpoint inhibitors was assembled based on current research to assess the expression profiles between the two patient cohorts [26].

Utilizing prior research from the open-access cancer-immunity database TIP (http://biocc.hrbmu.edu.cn/TIP/), we curated a gene list linked to favorable anti-PD-L1 treatment responses [27,28]. The GSVA method was employed to assess enrichment of cancer-immunity cycle genes and treatment-responsive signatures across risk groups stratified by our CRL-based scoring system. Correlations between risk score and immune-related gene profiles were visualized using the ggcor R package.

2.8 Analysis of Statistics

Group comparisons were performed using the Wilcoxon rank-sum test, with statistical significance set at $P < 0.05$. R was used for all bioinformatic analysis (v4.4.1).

3. Results

3.1 Discovery of an lncRNA Landscape Associated with Cuproptosis in Cervical Cancer

After the TCGA-CESC dataset's protein-coding transcripts were eliminated, 16,205 lncRNAs were left for co-expression analysis with the 16 cuproptosis genes that had previously been identified [9] (Figure 1A). After filtering, a panel of 188 lncRNAs linked to cuproptosis underwent univariate Cox screening (Figure 1B). The coefficient trajectories and cross-validation dynamics of six lncRNAs that showed significant relationships with patient outcome were plotted after they were advanced to LASSO regression (Figure 1C, D). A linear prognostic index was created by distilling four high-dimensional CRLs using multivariate Cox proportional - hazards modeling: AC096992.2 ($\beta = -0.5328$), MKLN1-AS ($\beta = 0.5597$), BAIAP2-DT ($\beta = 0.3912$), and LINC02356 ($\beta = -0.4509$). The risk score is equal to (-0.5328 × *AC096992.2 expression*) + (0.5597 × *MKLN*1-*AS expression*) + (0.3912 × *BAIAP*2-*DT expression*) + (-0.4509 × *LINC*02356 *expression*) . Strong connections between cuproptosis genes and the CRL quartet were found

by correlation profiling (Figure 1E), and there was a noticeable inter-correlation among the four lncRNAs (Figure 1F).

3.2 CESC Molecular Subtypes are Defined by Consensus Clustering

ConsensusClusterPlus divided CESC patients into two strong clusters based on cuproptosis-linked lncRNA expression: Cluster 1 exhibited a markedly elevated risk score ($P = 2.22\times10^{-16}$) (Figure 2A). Cluster 1 had considerably lower overall survival, according to survival interrogation using ClusterSurvival (Figure 2B, P=0.048). The four CRLs' varying expression across clusters and their relationships to clinicopathological factors were depicted in a heatmap (Figure 2C). KEGG pathway analysis revealed enrichment of oncogenic pathways—such as colorectal cancer, NSCLC, and homologous recombination—in cuproptosis-linked tumor biology (Figure 2D).

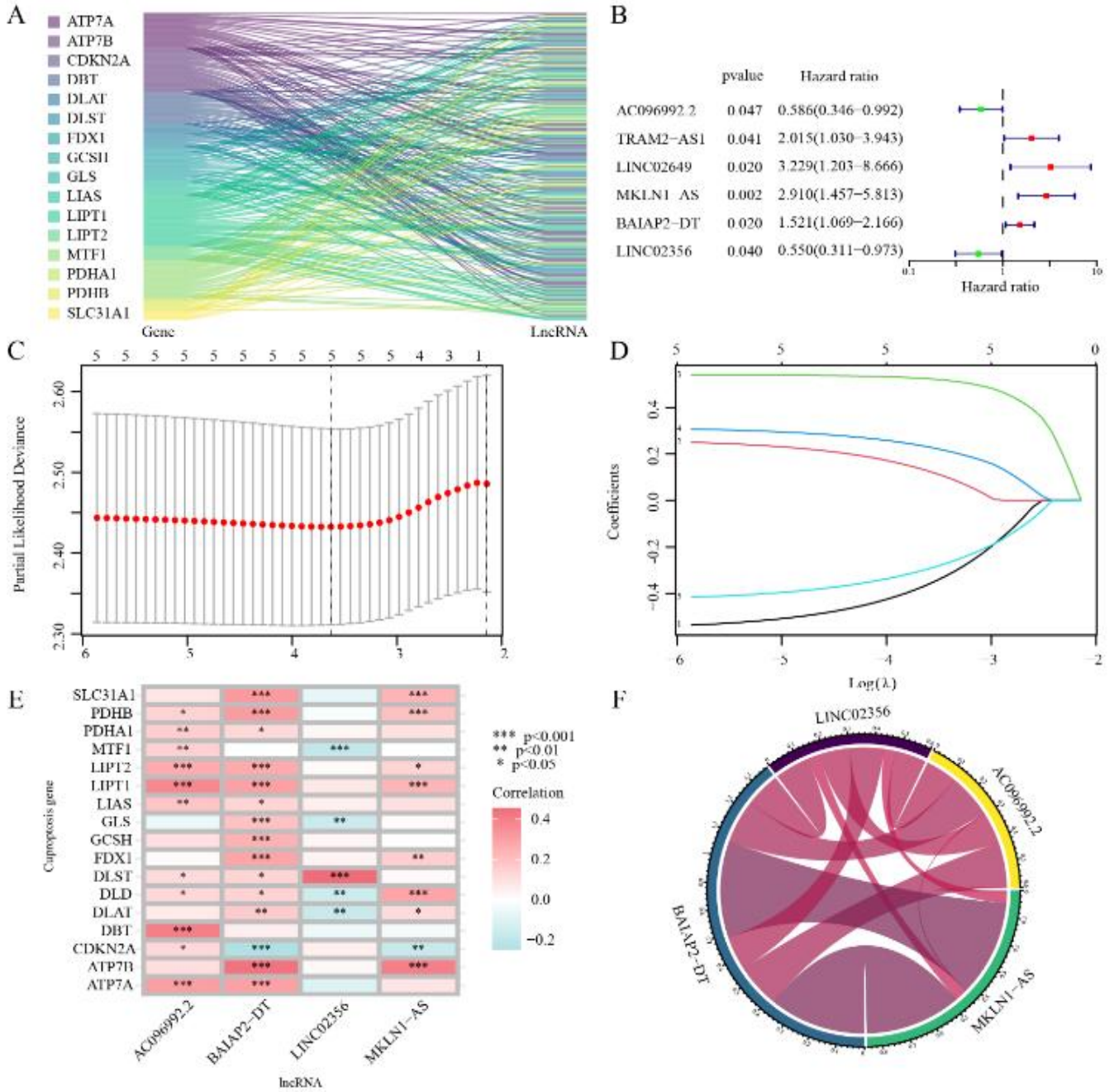

Figure 1: Identifying potential lncRNAs linked to cuproptosis. (A) Sankey diagram showing the co-expression of 188 CRLs and 16 cuproptosis genes. (B) Prognostic relationships of CRLs are evaluated using univariate Cox regression. (C) Ten-fold cross-validation to fine-tune the LASSO model's parameter selection. (D) Profiles of LASSO coefficients. (E) Correlation matrix between cuproptosis genes and the four chosen CRLs. (F) How the four CRLs relate to one another.
∗ P<0.05; ** P<0.01; *** P<0.001.

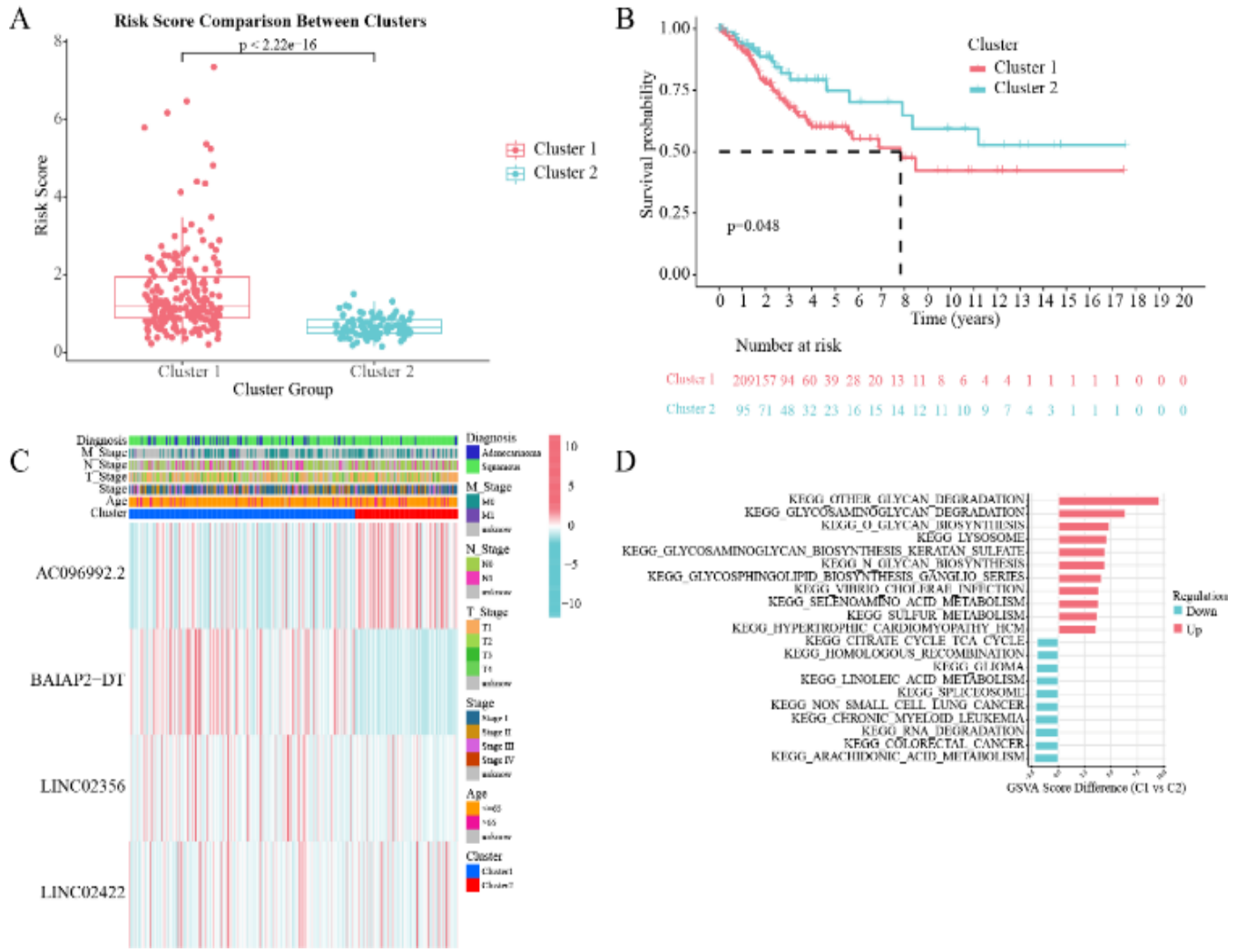

Figure 2: Consensus clustering for CESC molecular stratification. (A) The disparity in risk scores across the two clusters. (B) The disparity in overall survival across clusters. (C) Variations in the distribution of CRL expression and clinicopathologic characteristics among clusters. (D) The two-cluster comparison's KEGG enrichment profiles.

3.3 Verification of CRL Signatures and Their Prognostic Significance

According to the median risk score, patients were categorized into two categories, designated as low-risk and high-risk. While the high-risk group exhibited upregulated MKLN1-AS and BAIAP2-DT, the low-risk cohort showed elevated AC096992.2 and LINC02356 expression (Figure 3A). Mortality escalated consistently as risk scores rose for the entire cohort (Figure 3B, 3C). Among the overall patient population, individuals classified as high risk exhibited poorer outcomes compared to their low-risk counterparts (Figure 3D). The group was subsequently partitioned into two subgroups randomly in a 1:1 ratio: training (n = 152) and testing (n = 152) subgroups. This prognostic robustness persisted in both training (Figure 3E) and testing (Figure 3F) subsets. Time-dependent ROC analysis confirmed high specificity and sensitivity, yielding AUCs of 0.698, 0.708, and 0.725 for the entire population at 1, 3, and 5 years (Figure 3G). The four-CRL model demonstrated robust predictive efficacy, yielding AUCs of 0.783, 0.747, and 0.748 in the training set (Figure 3H) and 0.660, 0.676, and 0.731 in the testing set (Figure 3I).

3.4 Principal Component Analysis of the High-expression Genes, Cuproptosis Genes, Cuproptosis-related Lncrnas, and CRL Signatures

Four different gene sets were used for PCA: the high-expression genes, cuproptosis genes, cuproptosis-related lncRNAs, and CRL signatures. The findings indicated that the CRL-derived lncRNAs most effectively distinguished high- from low-risk patients, reinforcing their classification potential (Figure 4A–D). These results highlight the CRL signature's greater discriminatory ability.

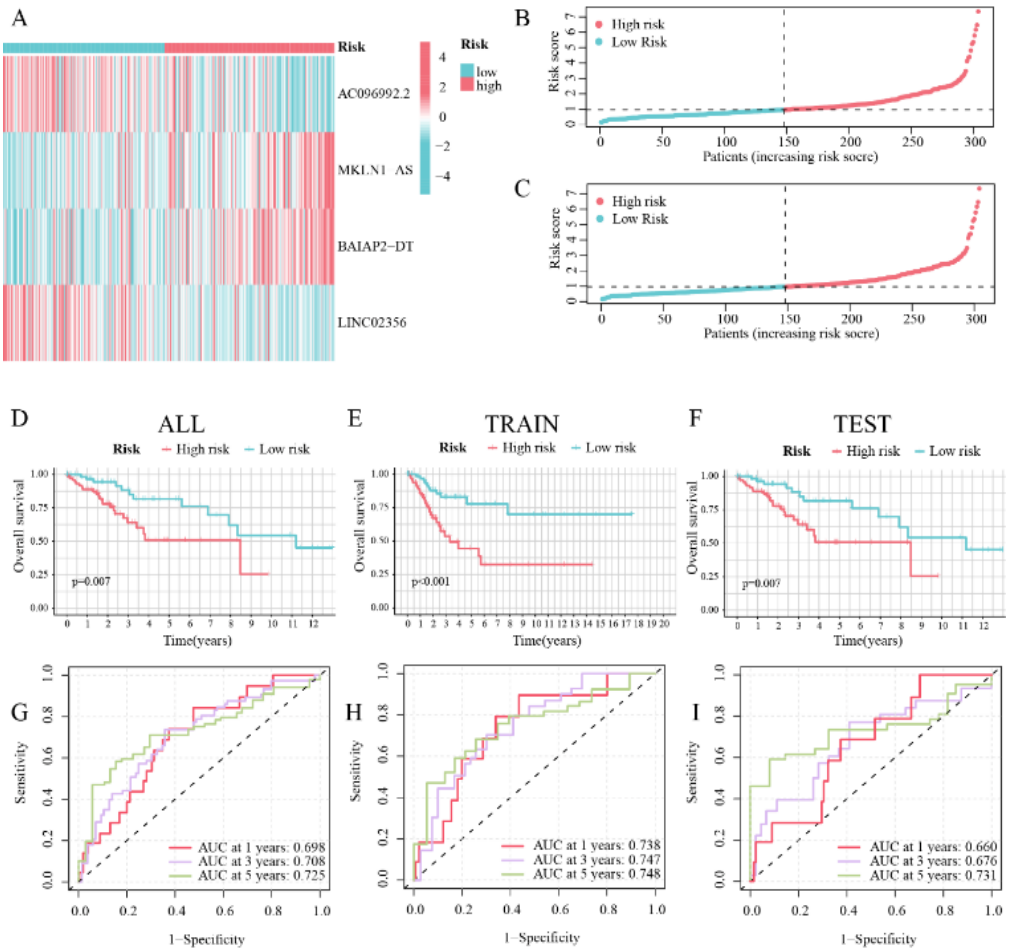

Figure 3: CRL signature validation for prognostic prediction. (A) The differential expression of the four CRLs between the two groups. (B) Distribution of risk scores among CESC patients. (C) Risk score and patient survival time correlation. (D) TCGA cohort-wide Kaplan-Meier survival curve. (E) The training TCGA subset's Kaplan-Meier survival curve. (F) The testing TCGA subset's Kaplan-Meier survival curve. (G) The entire TCGA cohort's time-dependent ROC curves. (H) The training subset's time-dependent ROC curves. (I) The testing subset's time-dependent ROC curves.

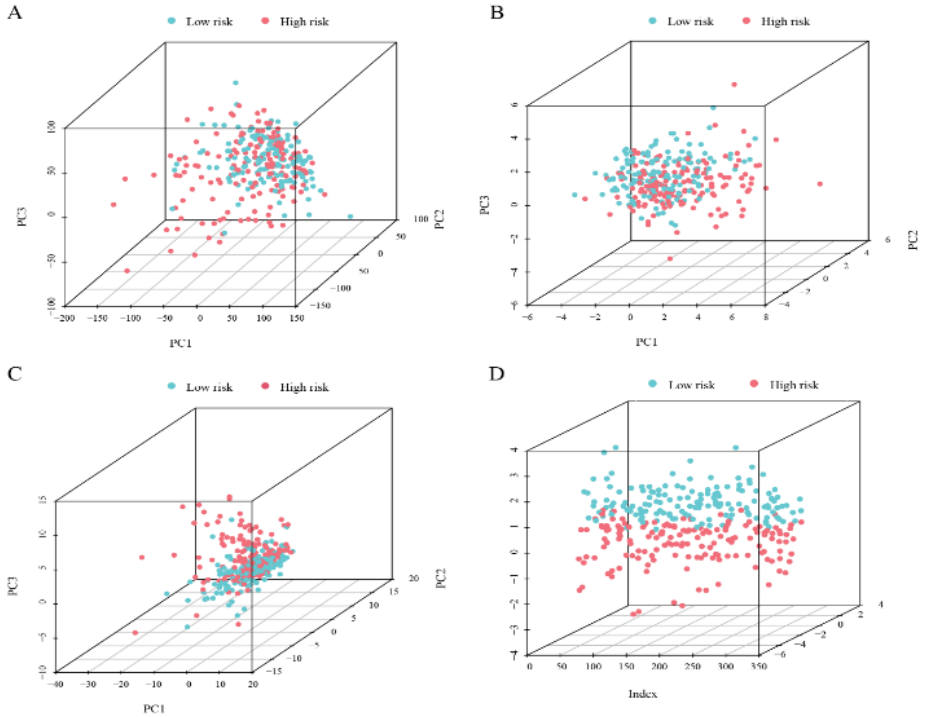

Figure 4: The CRL signature enables improved differentiation between high-risk and low-risk patients. (A) A PCA plot based on all genes with high expression. (B) A PCA plot based on genes linked to cuproptosis. (C) A PCA plot made from lncRNAs associated with cuproptosis. (D) A PCA plot based on the four-CRL prognostic model.

3.5 Clinical Subgroup Analysis of the CRL Risk Model

The heatmap illustrated that the variance of various clinicopathologic parameters, such as age, FIGO stage, histologic diagnosis, TNM stage, and risk score, was markedly affected by the four CRLs across risk groups in all TCGA cervical cancer samples (Figure 5A). Subsequently, patients were classified according to age (> 65 versus ≤ 65 years), histological type (adenocarcinoma versus squamous), pathological stage, and TNM classification. Survival was compared within each subgroup (Figure 5B–M). In all other categories, high-risk people exhibited markedly inferior overall survival compared to low-risk patients, with the exception of subgroups with limited sample sizes (adenocarcinoma, stage III–IV, N0, and M1). This finding suggests that our CRL risk model can effectively predict the prognosis of various clinical subgroups of CESC.

3.6 A Nomogram That Includes Risk Score and Clinicopathologic Factors

Univariate Cox found the risk score and N stage as significant predictors (Figure 6A), whereas multivariate Cox validated the risk score's independent prognostic strength (Figure 6B). The four-lncRNA model's clinical value was expanded by creating a nomogram that included age, stage, histology, TNM stage, and the CRL risk score, which accurately predicted 1-, 3-, and 5-year survival probabilities (Figure 6C). In predicting the prognosis of CESC, the CRL risk model (AUC = 0.698) performed better than conventional clinicopathologic markers (Figure 6D, E).

3.7 CRL-based Prognostic Signature Enrichment Profiling

To identify relationships between the risk score and biological mechanisms or signaling cascades, GO and KEGG enrichment analyses were utilized. While KEGG pathways were filtered at $FDR < 0.15$ and $P.adj < 0.05$, significant GO keywords were kept at $FDR < 0.05$ and $P.adj < 0.05$. The resulting enrichments showed close connections between the four CRLs and several functional modules, including TNF signaling, IL-17 signaling, extracellular matrix organization, and cytokine activity modulation (Figure 7A, B, C, D).

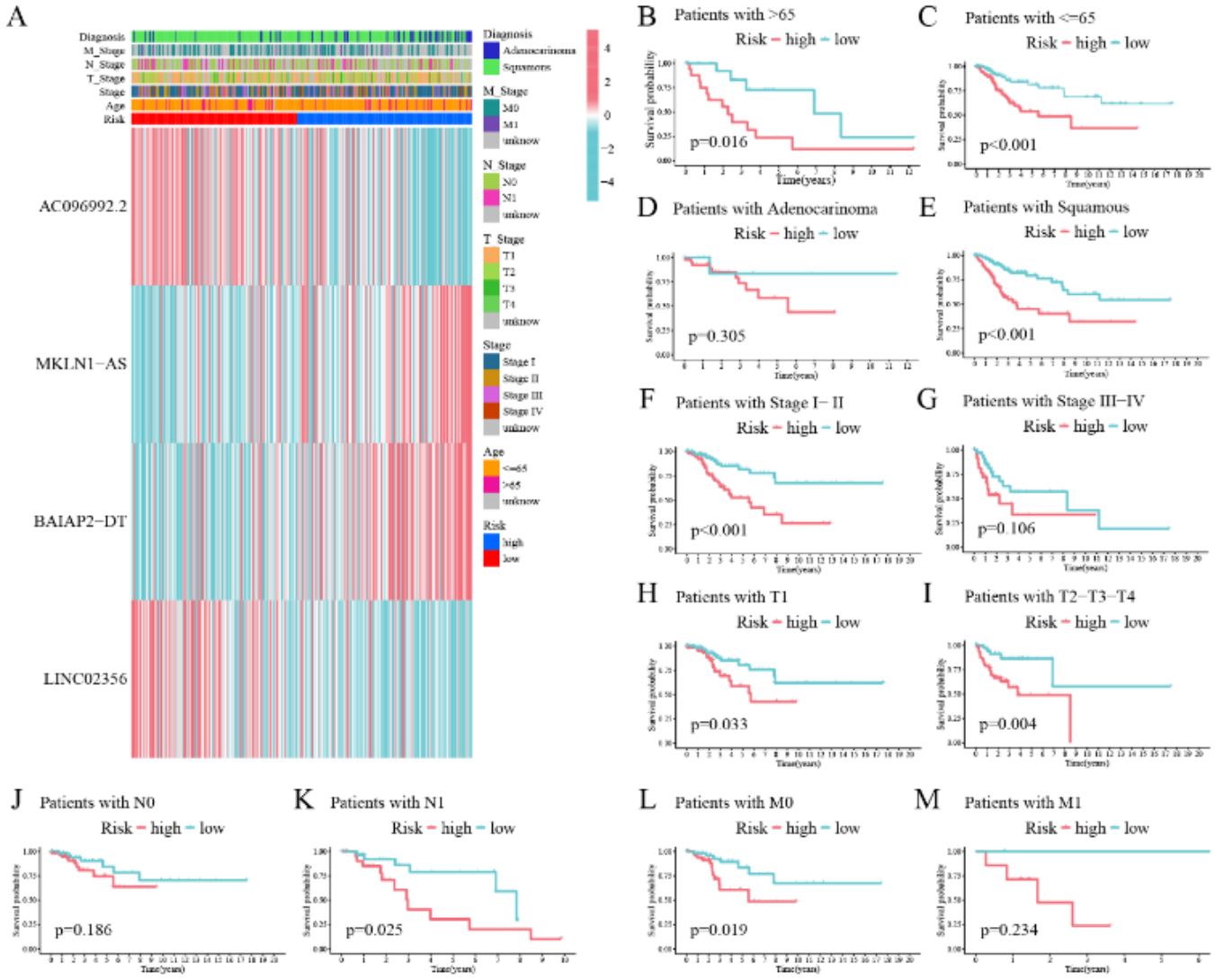

Figure 5: The CRL risk model's prognostic performance for each clinical subtype of CESC. (A) Heatmap showing the relationship between clinicopathologic factors and risk score. For (B) age > 65 years; (C) age <= 65 years; (D) adenocarcinoma; (E) squamous cell carcinoma; (F) stage I–II; (G) stage III–IV; (H) T1; (I) T2–T4; (J) N0; (K) N1; (L) M0; (M) M1, Kaplan–Meier survival curves categorized by the CRL signature.

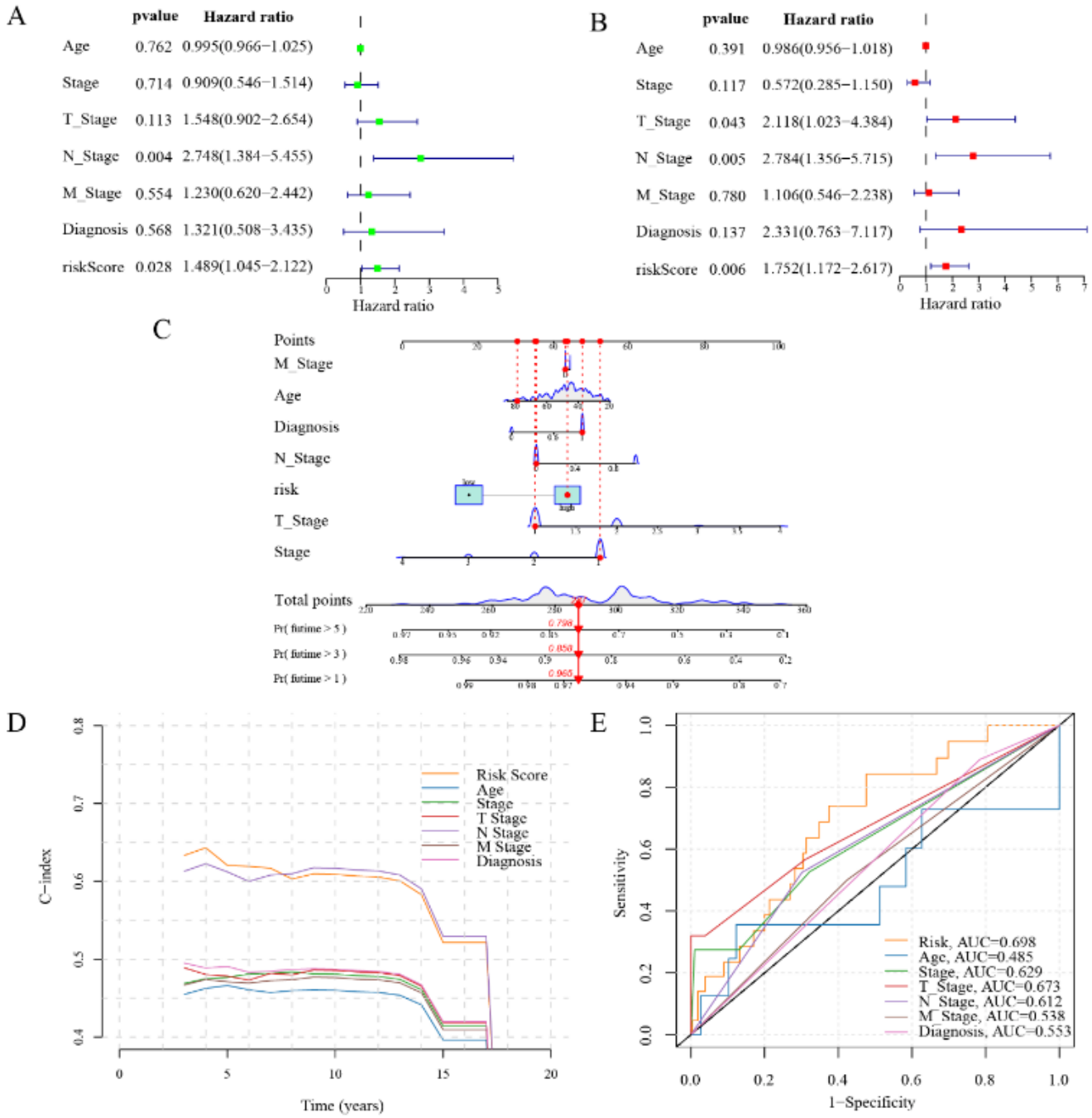

Figure 6: Assessment of the independent predictive significance of the CRL risk score alongside clinical and pathological characteristics. (A) Univariate Cox regression for clinical factors and risk score. (B) The forest plot of multivariate Cox regression's forest plot validates the risk score as an independent predictor. (C) Nomograms estimate 1-year, 3-year, and 5-year overall survival in CESC patients by combining the CRL risk score with clinical characteristics. (D) Concordance-index curves that contrast the risk score's prediction accuracy with traditional clinical characteristics. (E) ROC analysis assessing the risk score's discriminatory performance in relation to specific clinicopathologic parameters.

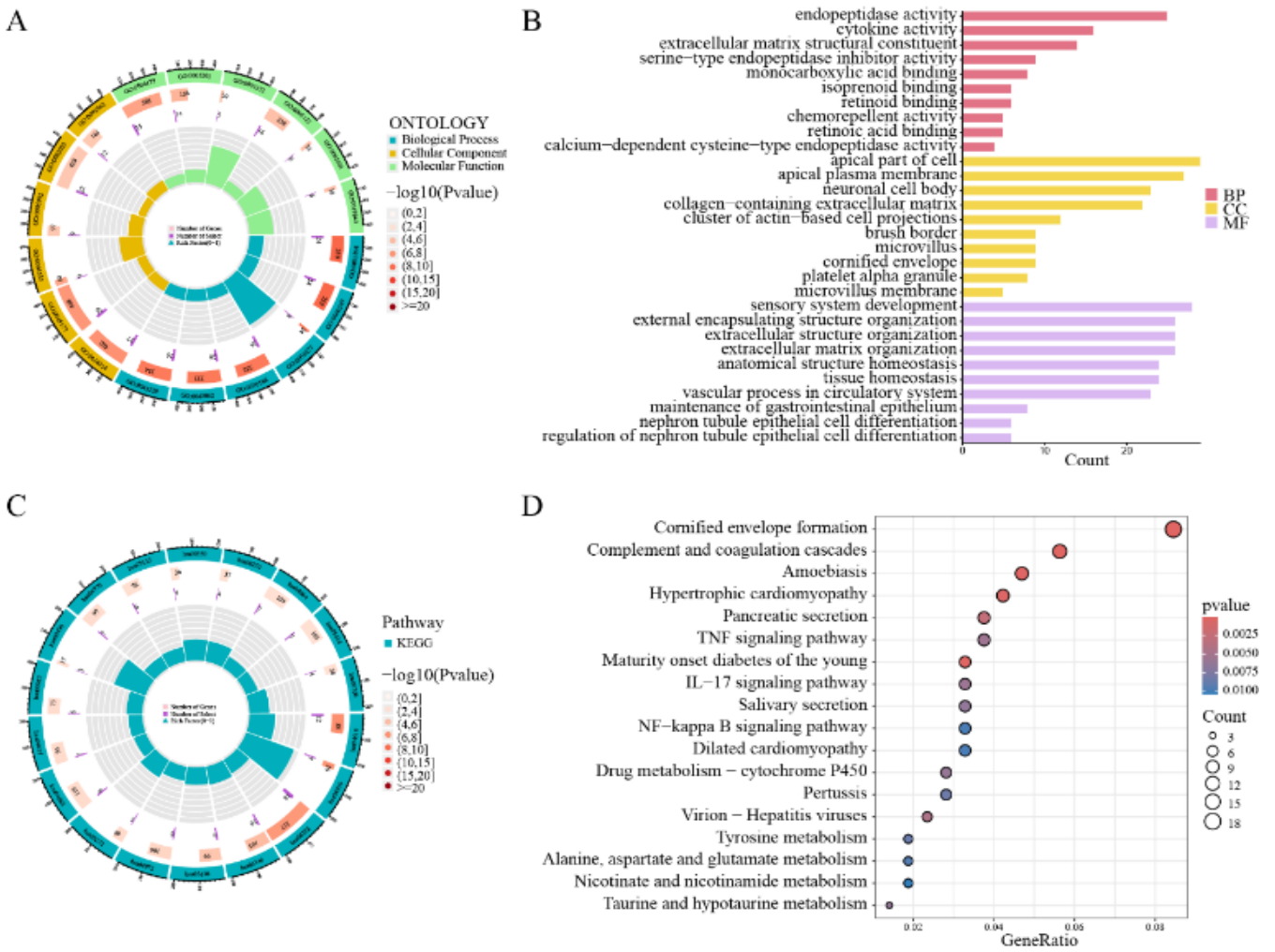

Figure 7: Pathway enrichment analysis utilizing the KEGG and GO. (A) Circos map showing the GO signaling pathways that rank highest. (B) The top GO pathways are divided into three categories: molecular function (MF), cellular component (CC), and biological process (BP). (C) Circos plot showing the main pathways of KEGG signaling. (D) The top KEGG-enriched pathways in a bubble plot.

3.8 Tumor Microenvironment and Immune Cell Infiltration can be Predicted by the CRL Risk Score

The CRL model has been previously associated with tumor microenvironment (TME) remodeling through GO enrichment analysis. We subsequently analyzed the correlation between the tumor immunity and CRL score, as the immunological elements of the tumor microenvironment considerably influence prognosis [29]. CIBERSORT initially assessed the association between 22 tumor-infiltrating immune cell (TIIC) subgroups and the risk score (Figure 8A). A comparative analysis revealed substantial differences between the low- and high-risk groups (Figure 8B). CD8+ T cells exhibited the most significant variations, indicating that CRLs predominantly influence the quantity and functionality of CD8+ T cells.

Concurrently, we analyzed the gene expression of immune checkpoints. The presence of several checkpoint genes varied among risk groups, and immune-checkpoint blockage is essential for the treatment of cervical cancer. The low-risk cohort exhibited elevated expression levels of all significantly altered checkpoints, including CD48, TNFRSF25, LAG3, CTLA4, BTLA, and IDO2 (Figure 8C). Specifically, CD8+ T-cell activation and proliferation are associated with elevated TNFRSF25 [30,31]. Patients with elevated TNFRSF25 showed enhanced CD8+ T-cell infiltration, low-risk classification, and a better prognosis, as expected by the CRL signature.

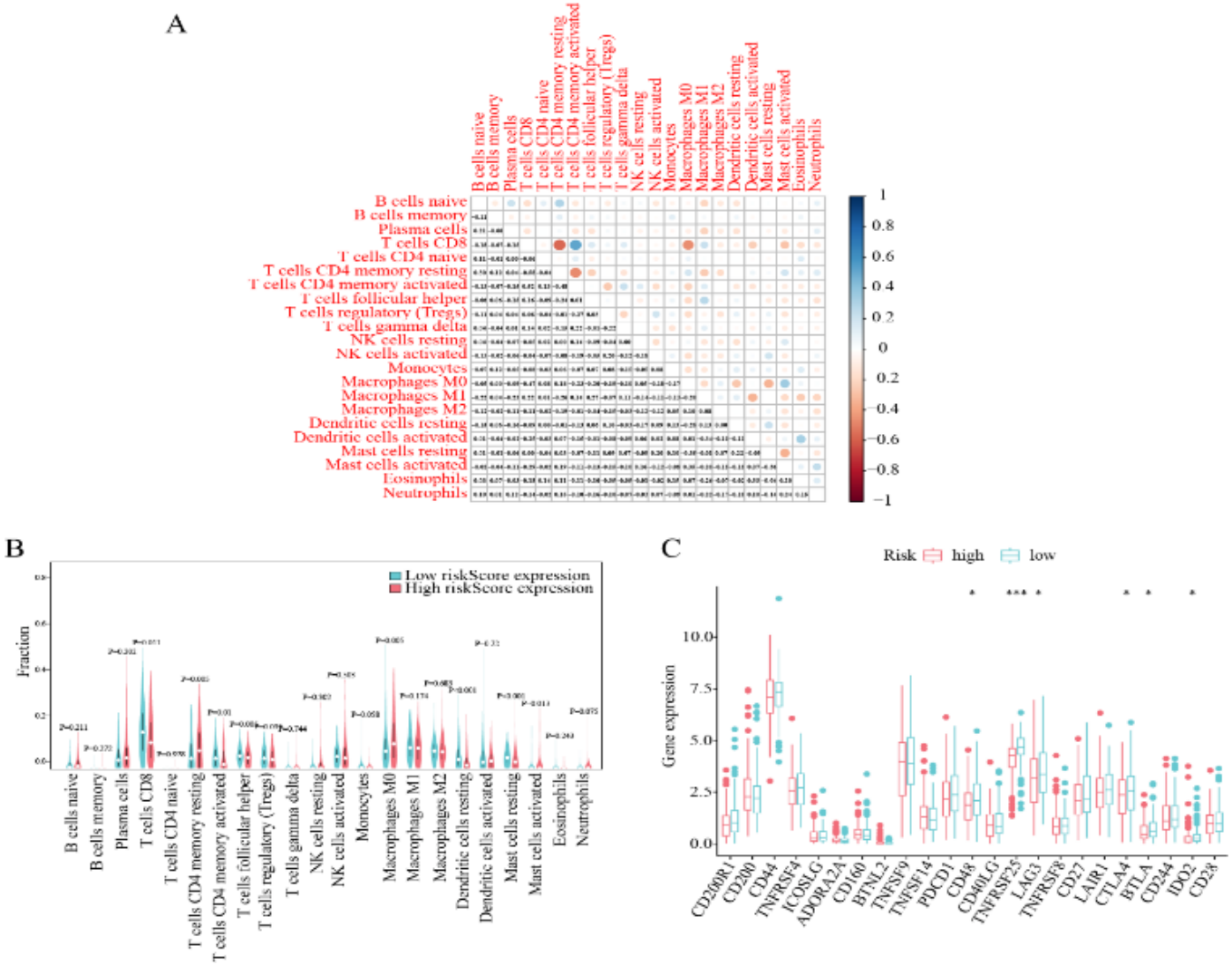

Figure 8: The tumor microenvironment and immunotherapeutic response are predicted by the CRL-derived risk score. (A) A bubble plot depicting the associations between the CRL risk score and immune cell populations. (B) Variations in immune cell infiltration profiles across the two groups. (C) Variations of immune checkpoint molecule expression across two groups.

3.9 The CRL Risk Score Predicts Divergent Immune Functional Landscape

We investigated immune function in CESC patients, as the risk score enables physicians to tailor immunotherapeutic protocols according to each patient's distinct checkpoint-gene expression profile. In comparison to the high-risk group, the low-risk group demonstrated enhanced immune activity, even while the low-risk subgroup exhibited an enhanced expression of immune-checkpoint genes (Figure 9A, B). Notably, immunosuppressive mechanisms such as T-cell and APC co-inhibition were incorporated into these heightened activities, indicating that diminishing suppressive signals may improve prognosis in the low-risk cohort. This idea was supported by the Tumor Immune Dysfunction and Exclusion (TIDE) algorithmic profiling, which showed that the low-risk group had significantly higher TIDE scores than the high-risk group ($P<0.01$) (Figure 9C). It indicates that immune-checkpoint inhibitors may be especially helpful for low-risk patients.

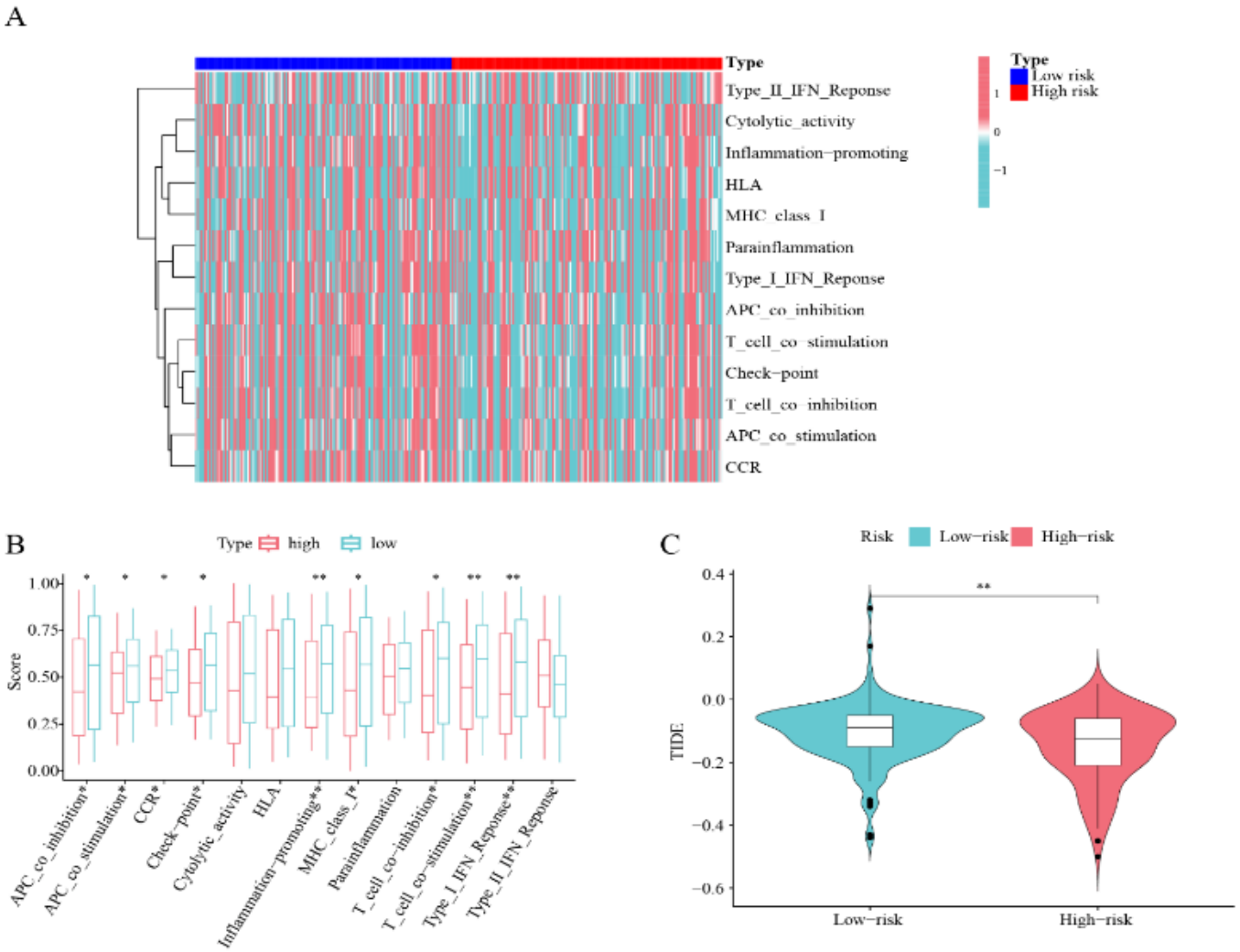

Figure 9: Immunotherapy can be guided by the CRL risk score, which predicts immune functional divergence. Variations in immune functional activity across two groups (A, B). Comparative analysis of TIDE scores between cohorts categorized as high and low risk. ∗ $P < 0.05$; ∗∗ $P < 0.01$; ∗∗∗ $P < 0.001$.

4. Discussion

Cervical cancer, the fourth most prevalent gynecological malignancy worldwide, significantly contributes to cancer-related mortality among women, posing a substantial threat to women's health [1]. Cervical cancer remains the second greatest cause of cancer-related mortality among women aged 20-39 in the United States, with incidence among those aged 30-44 rising by 1-2 percent per year [32,33]. Consequently, there is an imperative demand for more effective screening and therapeutic approaches. The prognosis remains unfavorable despite progress in conventional therapies, particularly for patients with advanced illness. The circumstance underscores the necessity for dependable biomarkers and feasible therapeutic targets.

Reliance on any one biomarker for CESC prognosis is prone to inaccuracy, much like the drawbacks of single-gene predictors. In contrast to single-biomarker models, composite models derived from multiple linked genes exhibit greater accuracy in prognostic predictions and substantially influence personalized cancer treatment. Cuproptosis is a copper-dependent cell death mechanism that has recently attracted much interest because of its potential for therapeutic use [9]. Cytotoxicity brought on by copper homeostasis can prevent the growth of cancerous cells, overcome resistance to chemotherapy, and allow for the targeted destruction of cancerous cells during immunotherapy [34-36]. Examining CRLs in CESC may clarify oncogenic pathways, aid in early identification, enhance risk stratification, and increase survival because long non-coding RNAs are associated with tumor proliferation, invasion, and metastasis [37].

We created a four-CRL model (AC096992.2, MKLN1-AS, BAIAP2-DT, and LINC02356) that defines the immunological landscape associated with CESC and independently predicts its prognosis. These lncRNAs were validated as independent prognostic indicators through LASSO and multivariate Cox analysis, which also accurately stratified patients into two risk categories. Several members of this quartet have been assigned oncogenic or tumor-suppressive roles in previous reports: MKLN1-AS promotes pancreatic cancer progression via the miR-185-5p/TEAD1 axis, BAIAP2-DT correlates with breast cancer outcome, and AC096992.2 is an established prognostic indicator in cervical cancer [38-40]. According to ROC and calibration curves, the excellent prediction accuracy of the four-CRL model was validated. The prediction potential of the signature was augmented through combining it with clinical data into a nomogram, which provided a valuable tool

for predicting patient prognosis in CESC.

Encircling neoplastic cells, the tumor microenvironment (TME) is a dynamic, multicellular ecosystem that includes vascular networks, cancer-associated fibroblasts, endothelial cells, extracellular matrix, soluble mediators, and immunological subsets such as T lymphocytes and macrophages [41]. Tumor-infiltrating immune cell (TIIC) density and immune-checkpoint molecule (ICI) expression characterize the immunological compartment, which has become a crucial biomarker and predictor of immunotherapeutic success in this context [42,43].

When TIICs from two risk-CRL groups were compared, the abundance of $CD8^+$ T cells showed a notable difference. Cervical squamous cell carcinoma prognosis can be independently predicted by $CD8^+$ T lymphocytes, the primary effectors of anti-tumor immunity [44,45]. The preclinical data showing that TNFRSF25 agonism activates and increases $CD8^+$ T cells, producing strong anti-tumor responses in mouse models, is consistent with the observed higher level of $CD8^+$ T cells within the group of low-risk [46]. It suggests that patients with a low risk exhibited heightened infiltration of $CD8^+$ T-cells, presumably attributable to the association between elevated TNFRSF25 and TNFRSF4 levels and the proliferation and activation of $CD8^+$ T-cells [30].

Crucially, immune-checkpoint blocking is anticipated to be more beneficial for low-risk people, as indicated by the CRL signature. Therefore, the four-CRL model improves prognostication and helps guide focused and customized immunotherapeutic approaches for CESC, which may lead to better clinical results.

Our research is clinically significant for forecasting the prognosis and therapy options for CESC patients; yet, it has obvious limitations. Validation was limited to publicly accessible TCGA data, and inter-patient variation may affect the four-CRL model's performance. Predictive robustness is supported by in silico analysis; nevertheless, comprehensive in vitro and in vivo investigations are essential to elucidate the molecular foundations of these correlations. As normal cervical tissue is rarely obtained clinically, our study lacks patient - derived sample validation. If adequate clinical samples are collected, we'll conduct the missing experimental validation.

5. Conclusion

We identified cuproptosis-associated lncRNAs to be a prospective prognostic biomarker and a possible approach for treatment in cervical squamous cell carcinoma. Clinicians may now discern patients who are most likely to benefit from immunotherapy or cytotoxic treatments and tailor precision care utilizing a 4-CRL model that reliably predicts patient outcomes and delineates immunological context.

References

[1] Bray F, Laversanne M, Sung H, et al. Global cancer statistics 2022: GLOBOCAN estimates of incidence and mortality worldwide for 36 cancers in 185 countries. CA: A Cancer Journal for Clinicians. 2024;74(3):229-263. doi:10.3322/caac.21834

[2] Abu-Rustum NR, Yashar CM, Arend R, et al. NCCN Guidelines® Insights: Cervical Cancer, Version 1.2024. Journal of the National Comprehensive Cancer Network. 2023;21(12):1224-1233.

[3] Xu M, Cao C, Wu P, Huang X, Ma D. Advances in cervical cancer: current insights and future directions. Cancer Communications. 2024;45(2):77-109. doi:10.1002/cac2.12629

[4] Gavinski K, DiNardo D. Cervical Cancer Screening. Medical Clinics of North America. 2023; 107(2): 259-269. doi:10.1016/j.mcna.2022.10.006

[5] Sun Q, Wang L, Zhang C, Hong Z, Han Z. Cervical cancer heterogeneity: a constant battle against viruses and drugs. Biomarker Research. 2022; 10(1) doi:10.1186/s40364-022-00428-7

[6] Yao S, Zhao L, Chen S, et al. Cervical cancer immune infiltration microenvironment identification, construction of immune scores, assisting patient prognosis and immunotherapy. Frontiers in Immunology. 2023;14doi:10.3389/fimmu.2023.1135657

[7] Liu C, Li X, Huang Q, et al. Single-cell RNA-sequencing reveals radiochemotherapy-induced innate immune activation and MHC-II upregulation in cervical cancer. Signal Transduction and Targeted Therapy. 2023;8(1) doi:10.1038/s41392-022-01264-9

[8] Zhang Y, Zhu J, Hu K, Qiu J, Zhang F. Multi-omics analyses construct an inflammatory response based prognostic gene signature for cervical cancer and suggest tumor infiltrating monocytes subgroups as key players. Frontiers in Immunology. 2025; 16 doi:10.3389/fimmu.2025.1563593

[9] Tsvetkov P, Coy S, Petrova B, et al. Copper induces cell death by targeting lipoylated TCA cycle proteins. Science. 2022; 375(6586): 1254-1261. doi:10.1126/science.abf0529

[10] Chen L, Min J, Wang F. Copper homeostasis and cuproptosis in health and disease. Signal Transduction and Targeted Therapy. 2022; 7(1) doi:10.1038/s41392-022-01229-y

[11] Xiao Y, Yin J, Liu P, Zhang X, Lin Y, Guo J. Triptolide-induced cuproptosis is a novel antitumor strategy for the treatment of cervical cancer. Cellular & Molecular Biology Letters. 2024; 29(1) doi:10.1186/s11658-024-00623-4

[12] Jin Y, Wu Q, Pan S, et al. Baicalein enhances cisplatin sensitivity in cervical cancer cells by promoting cuproptosis through the Akt pathway. Biomedicine & Pharmacotherapy. 2024; 179 doi:10.1016/j.biopha.2024.117415

[13] Herman AB, Tsitsipatis D, Gorospe M. Integrated lncRNA function upon genomic and epigenomic regulation. Molecular Cell. 2022;82(12):2252-2266. doi:10.1016/j.molcel.2022.05.027

[14] Tan YT, Lin JF, Li T, Li JJ, Xu RH, Ju HQ. LncRNA-mediated posttranslational modifications and reprogramming of energy metabolism in cancer. Cancer Communications. 2020; 41(2): 109-120. doi:10.1002/cac2.12108

[15] Bridges MC, Daulagala AC, Kourtidis A. LNCcation: lncRNA localization and function. Journal of Cell Biology. 2021; 220(2) doi:10.1083/jcb.202009045

[16] Bhan A, Soleimani M, Mandal SS. Long Noncoding RNA and Cancer: A New Paradigm. Cancer Research. 2017; 77(15): 3965-3981. doi:10.1158/0008-5472.Can-16-2634
[17] Aalijahan Hamid, Saeid G. Long non-coding RNAs and cervical cancer. Experimental and Molecular Pathology. 2019;106:7-16. doi:10.1016/j.yexmp.2018.11.010
[18] Smyth GK. Linear Models and Empirical Bayes Methods for Assessing Differential Expression in Microarray Experiments. Statistical Applications in Genetics and Molecular Biology. 2004;3(1):1-25. doi:10.2202/1544-6115.1027
[19] Engebretsen S, Bohlin J. Statistical predictions with glmnet. Clinical Epigenetics. 2019; 11(1) doi:10.1186/s13148-019-0730-1
[20] Wilkerson MD, Hayes DN. ConsensusClusterPlus: a class discovery tool with confidence assessments and item tracking. Bioinformatics. 2010;26(12):1572-1573. doi:10.1093/bioinformatics/btq170
[21] Aran D, Hu Z, Butte AJ. xCell: digitally portraying the tissue cellular heterogeneity landscape. Genome Biology. 2017; 18(1) doi:10.1186/s13059-017-1349-1
[22] Li T, Fan J, Wang B, et al. TIMER: A Web Server for Comprehensive Analysis of Tumor-Infiltrating Immune Cells. Cancer Research. 2017; 77(21): e108-e110. doi:10.1158/0008-5472.Can-17-0307
[23] Finotello F, Mayer C, Plattner C, et al. Molecular and pharmacological modulators of the tumor immune contexture revealed by deconvolution of RNA-seq data. Genome Medicine. 2019; 11(1) doi:10.1186/s13073-019-0638-6
[24] Chen B, Khodadoust MS, Liu CL, Newman AM, Alizadeh AA. Profiling Tumor Infiltrating Immune Cells with CIBERSORT. Cancer Systems Biology. 2018: 243-259: chap Chapter 12. Methods in Molecular Biology.
[25] Newman AM, Liu CL, Green MR, et al. Robust enumeration of cell subsets from tissue expression profiles. Nature Methods. 2015;12(5):453-457. doi:10.1038/nmeth.3337
[26] Auslander N, Zhang G, Lee JS, et al. Robust prediction of response to immune checkpoint blockade therapy in metastatic melanoma. Nature Medicine. 2018; 24(10): 1545-1549. doi:10.1038/s41591-018-0157-9
[27] Xu L, Deng C, Pang B, et al. TIP: A Web Server for Resolving Tumor Immunophenotype Profiling. Cancer Research. 2018; 78(23): 6575-6580. doi:10.1158/0008-5472.Can-18-0689
[28] Mariathasan S, Turley SJ, Nickles D, et al. TGFβ attenuates tumour response to PD-L1 blockade by contributing to exclusion of T cells. Nature. 2018;554(7693):544-548. doi:10.1038/nature25501
[29] Xu Leia YL, b, Jin-Ke Lia, Wei-Xing Dua, Ru-Gui Lia, Jing Yanga, Jian Lia, Fang Lia, Hua-Bing Tana. Immune cells within the tumor microenvironment: Biological functions and roles in cancer immunotherapy. Cancer Letters. 2020; 470: 126-133. doi:10.1016/j.canlet.2019.11.009
[30] Schreiber TH, Wolf D, Bodero M, Gonzalez L, Podack ER. T Cell Costimulation by TNFR Superfamily (TNFRSF)4 and TNFRSF25 in the Context of Vaccination. The Journal of Immunology. 2012; 189(7): 3311-3318. doi:10.4049/jimmunol.1200597
[31] Lyu X, Zhao L, Chen S, et al. Targeting TNFRSF25 by agonistic antibodies and multimeric TL1A proteins co-stimulated CD8+T cells and inhibited tumor growth. Journal for ImmunoTherapy of Cancer. 2024; 12(8) doi:10.1136/jitc-2024-008810
[32] Siegel RL, Giaquinto AN, Jemal A. Cancer statistics, 2024. CA: A Cancer Journal for Clinicians. 2024; 74(1): 12-49. doi:10.3322/caac.21820
[33] Siegel RL, Miller KD, Wagle NS, Jemal A. Cancer statistics, 2023. CA: A Cancer Journal for Clinicians. 2023;73(1):17-48. doi:10.3322/caac.21763
[34] Xie J, Yang Y, Gao Y, He J. Cuproptosis: mechanisms and links with cancers. Molecular Cancer. 2023; 22(1) doi:10.1186/s12943-023-01732-y
[35] Liu WQ, Lin WR, Yan L, Xu WH, Yang J. Copper homeostasis and cuproptosis in cancer immunity and therapy. Immunological Reviews. 2023;321(1):211-227. doi:10.1111/imr.13276
[36] Wang Y, Chen Y, Zhang J, et al. Cuproptosis: A novel therapeutic target for overcoming cancer drug resistance. Drug Resistance Updates. 2024; 72 doi:10.1016/j.drup.2023.101018
[37] Wang X, Gu Y, Zhang L, Ma J, Xia Y, Wang X. Long noncoding RNAs regulate intrauterine adhesion and cervical cancer development and progression. Seminars in Cell & Developmental Biology. 2024; 154: 221-226. doi:10.1016/j.semcdb.2023.02.007
[38] Wen K WL, Su H, Yu L, Zhang S, Wei M, Wang Y, Zhao L, Guo Y. Development of a m6A- and ferroptosis-related LncRNA signature for forecasting prognosis and treatment response in cervical cancer. BMC Cancer. 2025 Mar 31 2025; 25: 580. doi:10.1186/s12885-025-13974-8
[39] Chen J LL, Feng Y, Zhao Y, Sun F, Zhou X, Yiqi D, Li Z, Kong F, Kong X. MKLN1-AS promotes pancreatic cancer progression as a crucial downstream mediator of HIF-1α through miR-185-5p/TEAD1 pathway. Cell Biol Toxicol. 2024 May 13 2024; 40: 30. doi:10.1007/s10565-024-09863-8
[40] Chen J LX, Yan S, Li J, Zhou Y, Wu M, Ding J, Yang J, Yuan Y, Zhu Y, Wu W. An autophagy-related long non-coding RNA prognostic model and related immune research for female breast cancer. Front Oncol. 2022 Dec 15 2022;12:929240. doi:10.3389/fonc.2022.929240
[41] Bilotta MT, Antignani A, Fitzgerald DJ. Managing the TME to improve the efficacy of cancer therapy. Frontiers in Immunology. 2022; 13 doi:10.3389/fimmu.2022.954992
[42] Arner EN, Rathmell JC. Metabolic programming and immune suppression in the tumor microenvironment. Cancer Cell. 2023; 41(3): 421-433. doi:10.1016/j.ccell.2023.01.009
[43] Wang Y, Peng L, Wang F. M6A-mediated molecular patterns and tumor microenvironment infiltration characterization in nasopharyngeal carcinoma. Cancer Biology & Therapy. 2024; 25(1) doi:10.1080/15384047.2024.2333590
[44] Raskov H, Orhan A, Christensen JP, Gögenur I. Cytotoxic CD8+ T cells in cancer and cancer immunotherapy. British Journal of Cancer. 2020; 124(2): 359-367. doi:10.1038/s41416-020-01048-4
[45] Shen X, Wang C, Li M, et al. Identification of CD8+ T cell infiltration-related genes and their prognostic values

in cervical cancer. Frontiers in Oncology. 2022; 12 doi:10.3389/fonc.2022.1031643

[46] Wu W, Chia T, Lu J, et al. IL-2Rα-biased agonist enhances antitumor immunity by invigorating tumor-infiltrating CD25+CD8+ T cells. Nature Cancer. 2023;4(9):1309-1325. doi:10.1038/s43018-023-00612-0